NANO LETTERS

pubs.acs.org/NanoLett Letter

Cellular Delivery of Large Functional Proteins and Protein−Nucleic Acid Constructs via Localized Electroporation

Nibir Pathak,[#] Cesar A. Patino,[#] Namrata Ramani, Prithvijit Mukherjee, Devleena Samanta, Sasha B. Ebrahimi, Chad A. Mirkin, and Horacio D. Espinosa*

Cite This: *Nano Lett.* 2023, 23, 3653−3660 Read Online

ACCESS | Metrics & More | Article Recommendations | Supporting Information

ABSTRACT: Delivery of proteins and protein−nucleic acid constructs into live cells enables a wide range of applications from gene editing to cell-based therapies and intracellular sensing. However, electroporation-based protein delivery remains challenging due to the large sizes of proteins, their low surface charge, and susceptibility to conformational changes that result in loss of function. Here, we use a nanochannel-based localized electroporation platform with multiplexing capabilities to optimize the intracellular delivery of large proteins (β-galactosidase, 472 kDa, 75.38% efficiency), protein−nucleic acid conjugates (protein spherical nucleic acids (ProSNA), 668 kDa, 80.25% efficiency), and Cas9-ribonucleoprotein complex (160 kDa, ∼60% knock-out and ∼24% knock-in) while retaining functionality post-delivery. Importantly, we delivered the largest protein to date using a localized electroporation platform and showed a nearly 2-fold improvement in gene editing efficiencies compared to previous reports. Furthermore, using confocal microscopy, we observed enhanced cytosolic delivery of ProSNAs, which may expand opportunities for detection and therapy.

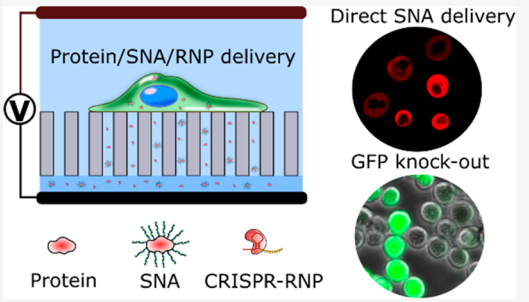

KEYWORDS: *protein delivery, spherical nucleic acids, localized electroporation, CRISPR gene editing*

The introduction of exogenous proteins into cells enables the analysis and manipulation of cellular functions such as the perturbation of intracellular signaling pathways,[1] genome editing,[2,3] regulation of gene expression,[4,5] and intracellular sensing.[6,7] These capabilities can be leveraged to treat diseases or to elucidate fundamental mechanisms of the cell's complex machinery. There are several key approaches for the delivery of functional proteins into cells, including physical membrane disruption systems (e.g., electroporation,[8−12] cell squeezing,[13−15] and hydroporation[16,17]), exogenous transfection reagents (e.g., lipid vesicle carriers[18,19]), chemical modifications of protein surfaces (e.g., protein spherical nucleic acids,[20,21] cell penetrating peptides,[22] hydrophobic modifications[23]), and polymer based carriers.[24,25] However, due to the large variation in protein size, surface charge, and structure, there are advantages and disadvantages for each platform depending on the characteristics of the protein and application of interest. For instance, while it has been shown how polymers can be functionalized to carry a range of proteins and peptides into the cytosol, they can also increase cytotoxicity and require extensive optimization to determine the necessary degree of functionalization.[26] In the context of *in vitro* studies, the physical delivery systems like electroporation provide more control over the dosage and the intracellular uniformity of the delivered protein.[27] Bulk electroporation is widely used due to ease of use and versatility but leads to low cell viability and unwanted genetic perturbation for sensitive cell types.[10] Moreover, delivery of large proteins with traditional electroporation-based systems is challenging because of the relatively small pore sizes generated across cell membranes as compared to other physical membrane disruption systems like microinjection and mechanoporation.[5,28,29] An additional challenge with electroporation systems is the diffusion-dominant molecular transport of weakly charged proteins, which contrasts the electrophoretic-dominant delivery of highly charged nucleic acids.[30] Therefore, to successfully deliver a particular protein with electroporation, several conditions must be met: (1) the size of the pores generated by the electric field must be greater than a certain threshold for the protein of interest to directly enter the cytosol; (2) the pores must remain open above this threshold size for enough time for delivery of proteins in sufficient quantity; (3) the structure of the protein must be preserved to retain its functional integrity; (4) the pores must reseal following delivery to prevent cell death. Extensive optimization of the electric pulse parameters (voltage amplitude, pulse shape, frequency, pulse duration, and number of pulses), in conjunction with other experimental

Received: November 7, 2022
Revised: February 22, 2023
Published: February 27, 2023

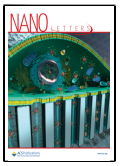

https://doi.org/10.1021/acs.nanolett.2c04374
Nano Lett. 2023, 23, 3653−3660

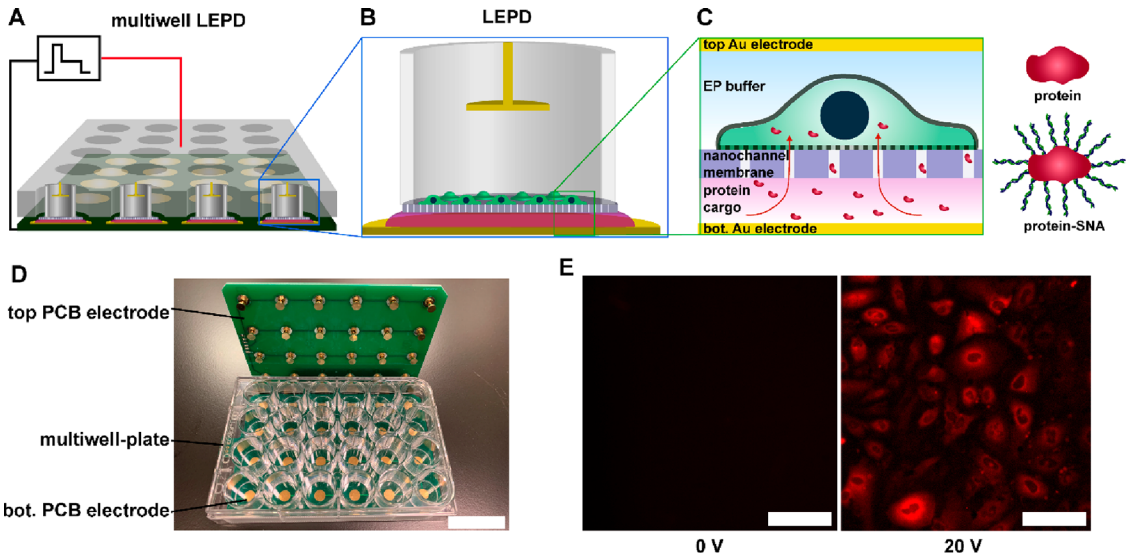

Figure 1. Multiwell LEPD architecture, localized electroporation mechanism, and intracellular delivery. Schematics of (A) multiwell LEPD system, (B) single LEPD containing cells, and (C) localized electroporation mechanism for protein delivery. (D) Photograph of physical multiwell LEPD assembly, which contains a top PCB electrode holder with Au stub pins, a bottomless multiwell plate, and a bottom PCB with Au pads. Scale bar = 40 mm. (E) Representative fluorescent micrographs of HeLa cells incubated (~20 s) with AF-647-tagged β-gal (472 kDa) proteins (left, control) and after electroporation-induced delivery of AF-647-tagged β-gal (right) with LEPD (~20 s pulse time). Scale bar = 70 μm.

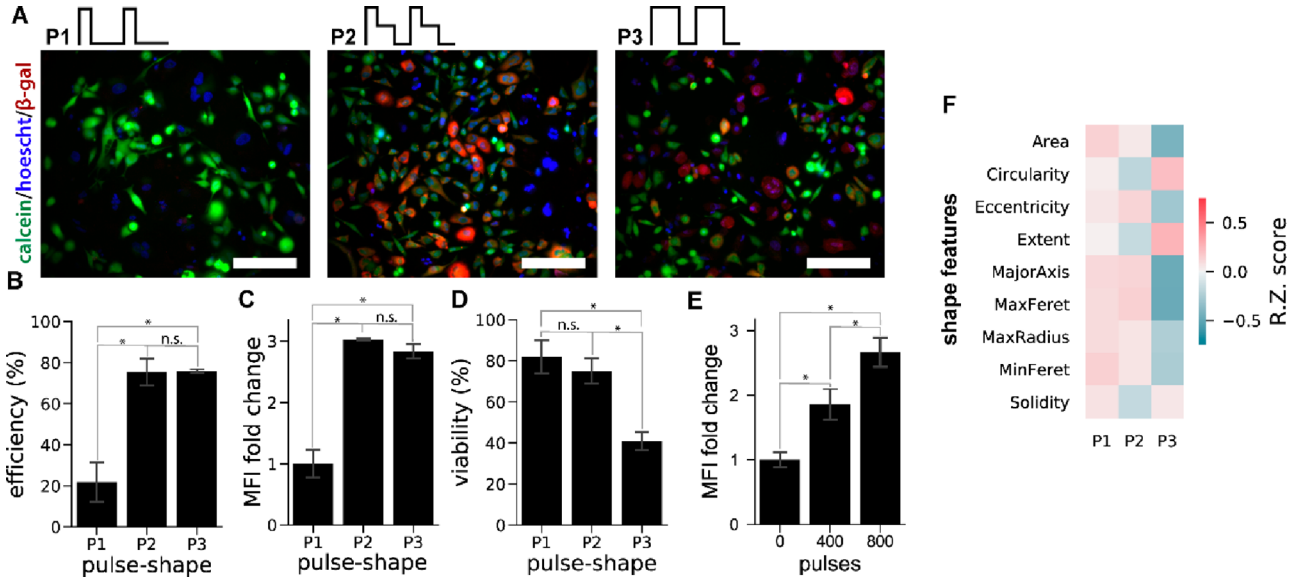

Figure 2. Delivery of a large protein and pulse shape optimization. (A) Composite fluorescent micrographs of HeLa cells stained with calcein-AM (green) viability marker and Hoechst (blue) nuclear marker following the delivery of β-gal-AF-647 (red) using short single-level pulses (P1, V = 20 V, t = 0.5 ms), bilevel pulses (P2, V_1 = 20 V, V_2 = 10 V, t_1 = 0.5 ms, and t_2 = 1.5 ms) and long single-level pulses (P3, V = 20 V, t = 2.0 ms). Scale bars = 100 μm. (B) Delivery efficiencies of β-gal corresponding to the various applied pulse shapes. (C) Mean fluorescence intensity (MFI) fold change of AF-647 normalized with respect to P1. (D) Viability percentages of the different pulse treatments. (E) Variation in protein dosage with pulse number as shown by the different levels of mean fluorescence intensity (MFI) fold change of intracellular β-gal normalized with respect to a zero-pulse control. (F) Heat-map of standardized scores (R.Z. score) of various cell-shape features used to compare morphological outcomes following β-gal delivery with the different pulse inputs. Error bars indicate standard error of the mean. N = 2 or 3 for all bar plots. *p < 0.05, **p < 0.01, n.s.= not significant.

factors such as electroporation buffer composition and protein concentration, is required to satisfy these conditions and achieve efficient cargo delivery.[8,9,30] Recently, we developed a well-plate based localized electroporation device (LEPD) designed for the multiplexing of pulse parameters and experimental conditions to expedite the optimization process needed to achieve efficient delivery of plasmids, oligonucleotides, and siRNA in a variety of cell types, including hard-to-transfect induced pluripotent stem cells, while retaining high cell viability.[8]

In this work, we used the multiwell plate LEPD to ascertain the efficient delivery of large proteins (hundreds of kDa) and identify pulse-shape and voltage amplitude parameters that optimize protein delivery. In contrast to some bulk electroporation systems, which come with preset electroporation conditions, the multiwell LEPD confers the user full

https://doi.org/10.1021/acs.nanolett.2c04374
Nano Lett. 2023, 23, 3653−3660

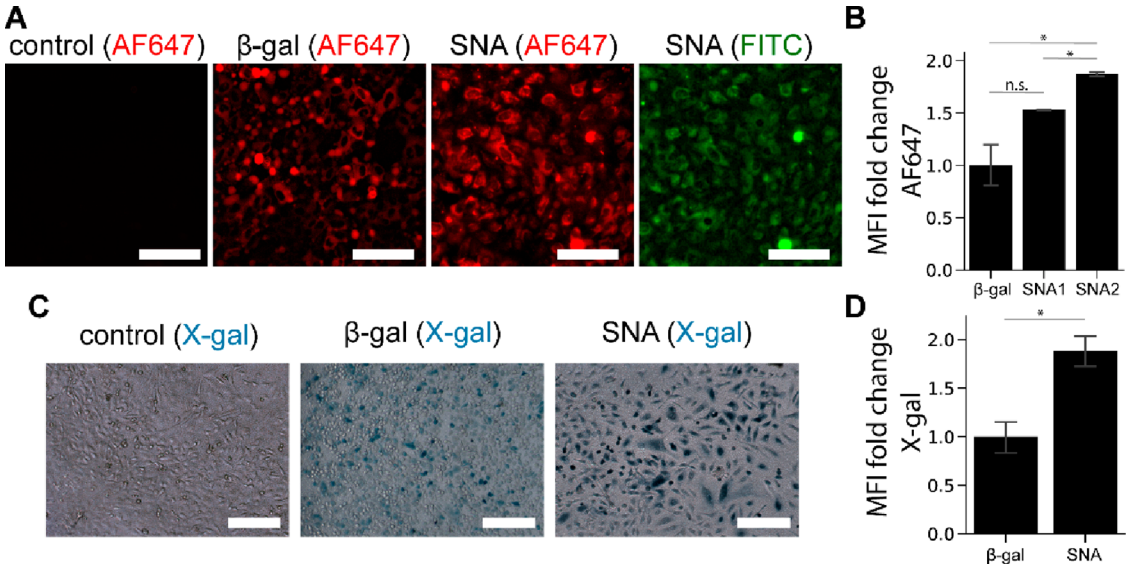

Figure 3. Delivery of ProSNA and protein activity assay. (A) Representative fluorescent micrographs of HeLa cells following 20 s incubation with AF-647-tagged β-gal-SNA (control), electroporation of AF-647-tagged β-gal, or electroporation of β-gal-SNA. The DNA on the β-gal-SNA is tagged with FITC. (B) Mean fluorescence intensity (MFI) fold change of AF-647 for different cargo under the same delivery conditions: β-gal (no DNA attached), SNA1 (β-gal-SNA with 18 DNA strands/ β-gal core), SNA2 (β-gal-SNA with 25 DNA strands/ β-gal core). (C) Representative images of electroporated HeLa cells, with blank samples (control), β-gal, and β-gal-SNA, after X-gal assay. (D) MFI fold change of X-gal blue precipitate comparing enzyme activity of bare β-gal and β-gal-SNA. Error bars indicate standard error of the mean, $N = 2$ or 3 and $^*p < 0.05$, n.s.= not significant. Scale bars = 100 μm.

experimental optimization capability. This can be exploited to individually tune experimental conditions, e.g., pulse characteristics, in the plethora of applications. Here, we demonstrate the efficient delivery of a large protein (β-galactosidase, β-gal, MW = 472 kDa), a protein densely surface-functionalized with DNA (protein spherical nucleic acid conjugate, ProSNA, MW = 668 kDa), and a ribonucleoprotein complex (Cas9-RNP, MW = 160 kDa). Furthermore, we used an automated imaging platform to acquire fluorescence images across the multiwell LEPD immediately following electroporation and employed a deep-learning and feature extraction pipelines to segment cells and obtain various morphological measurements from each well with single-cell resolution.[8,31−34]

To deliver protein cargoes into both adherent and suspension cell types while preserving function and viability, we utilized the multiwell LEPD and optimized the electroporation parameters. The LEPD design consists of a polycarbonate nanochannel membrane attached to a cell culture well (seeding capacity of ∼20 000−50 000 cells) that is placed in a multiwell plate with embedded gold electrodes (Figure 1A−D). Each row in the well-plate LEPD is individually addressable by a pulse generator with tunable parameters that include pulse shape, amplitude, frequency, and duration. Upon application of the electric pulses, the electric field is localized at the interface between the nanochannels (diameter = 400 nm) and the cell membrane, which results in the formation of hydrophilic pores in the cell membrane when the transmembrane potential (TMP) exceeds a threshold level (∼0.2−1 V).[35−37] The dynamic process of pore formation, expansion, and resealing is sensitive to several parameters including the TMP and membrane tension, which can be altered by tuning the electrical inputs and the cell culture conditions.[28,35] To investigate the system's capability for delivery of very large proteins, we selected Alexa Fluor 647 (AF-647) tagged β-gal (Figure 1E) as a model protein because of its large size and well-established activity assay. We also investigated the effect of charge by delivering β-gal-SNAs, which combine the functionality of both proteins and nucleic acids.[20,38,39]

First, we tested the effect of voltage amplitude and pulse-shape on the delivery of AF-647-tagged β-gal proteins into adhered HeLa cells. We applied pulse profiles of different shapes consisting of short single-level pulses (P1), bilevel pulses (P2), or long single-level pulses (P3) (Figure 2A, Figure S1). The applied voltage must be sufficiently high to yield a threshold TMP at the cell membrane to generate hydrophilic pores.[28] In our previous work where we delivered highly charged molecules like plasmids and nucleic acids, we found that an applied voltage amplitude of 20 V was enough to enable intracellular delivery while retaining viability.[8] Using a voltage amplitude of 20 V, we observed that the short single-level pulse (P1) resulted in the lowest percentage of cells with detectable signal (21.78%) and the lowest mean fluorescence intensity (MFI) of AF-647 (Figure 2B,C). Conversely, the bilevel pulse (P2) and the long single-level pulse (P3) profiles resulted in the successful delivery of β-gal in 75.38% and 75.86% of the cells, respectively, with significantly higher MFI of AF-647 compared to the short single-level pulses (P1). The rationale for applying a bilevel pulse was to supply a high enough voltage amplitude for a short duration (V_1 = 20 V, t_1 = 0.5 ms) to induce hydrophilic pore formation and follow it with a lower voltage (V_2 = 10 V, t_2 = 1.5 ms) to maintain the pores open for a longer duration to provide sufficient time for the weakly charged proteins to diffuse into the cytosol. This was done without subjecting the cells to strong electric fields that may result in joule heating or formation of reactive oxygen species, which can be deleterious and lead to cell death. Evidently, P3 (V_1 = 20 V, t_1 = 2.0 ms) resulted in a significant reduction in cell viability (40.88%) as opposed to 75.03% viability in the case of P2 (Figure 2D). Taken together, our results show that a bilevel pulse shape enables efficient delivery of β-gal protein while preserving the viability and functional

https://doi.org/10.1021/acs.nanolett.2c04374
Nano Lett. 2023, 23, 3653−3660

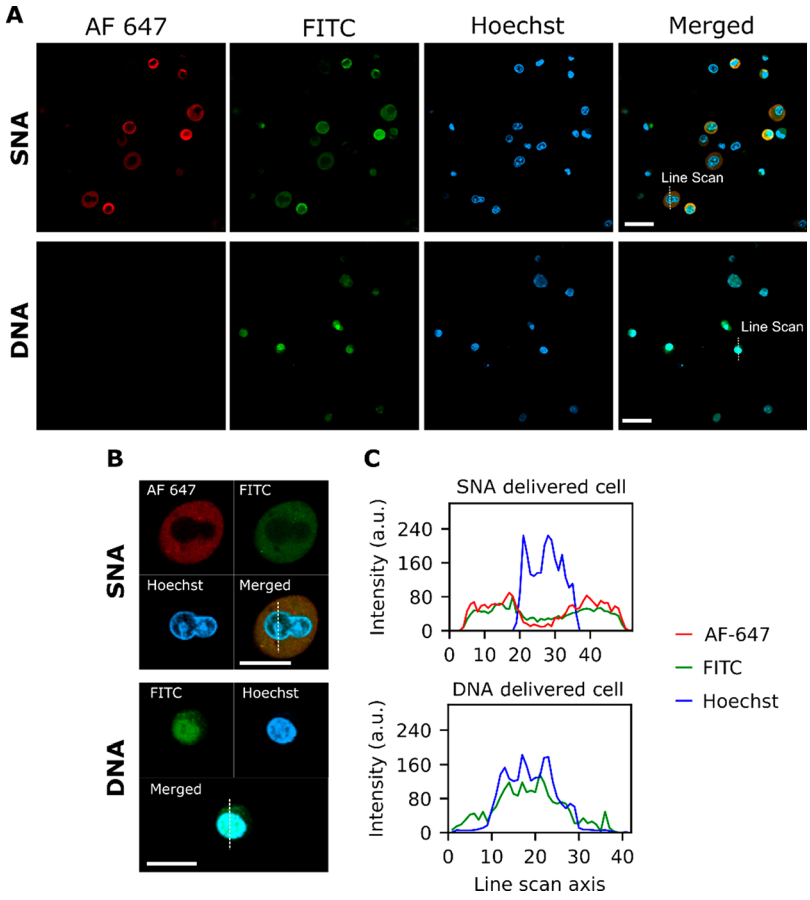

Figure 4. Intracellular localization analysis of ProSNAs and linear DNA. (A) Representative fluorescent micrographs obtained by confocal imaging of HeLa cells after delivery of AF647 conjugated β-gal-SNA (upper panel) and FITC tagged linear DNA (lower panel), respectively. Scale bar = 50 μm. (B) Zoomed in view of a representative cell delivered with ProSNA (top) and linear DNA (bottom), respectively. Scale bar = 25 μm. (C) Line scans of fluorescence intensities across representative β-gal-SNA delivered and linear DNA delivered cells. The DNA on the β-gal-SNA is tagged with FITC.

integrity of the cells. The effect of pulse shape was also tested for the delivery of β-gal-SNA, and we observed optimal delivery with P2 (Figure S2). To investigate protein delivery dosage into live cells, we adjusted the number of applied P2 pulses (Figure 2E) and observed a linear increase with pulse number. Additionally, we utilized an automated imaging platform equipped with deep-learning models for cell segmentation to analyze the morphological features of the cells following electroporation.[8] Briefly, we trained deep-learning models consisting of a U-Net architecture to segment individual cells in the images and employed an image profiling software (CellProfiler) to measure a variety of shape and intensity features (refer to Table S1 for descriptions of the shape features). To compare the morphological outcomes across experiments, we standardized each feature using the robust Z score (R.Z. score) and plotted a heatmap to visualize the differences (Figure 2F). The analysis revealed that a long pulse shape leads to significant shrinking and rounding of the cells, which is known to be detrimental to their normal function.[40] We note that the multiplexing capabilities of the multiwell LEPD platform made possible the expedited optimization of the pulse parameters necessary to deliver a large protein like β-gal (464 kDa) using the localized electroporation mechanism.

One robust method of enhancing cellular delivery of proteins is functionalizing protein cores with a dense shell of radially oriented nucleic acids to form protein spherical nucleic acids (ProSNAs).[20,38,39] ProSNAs readily enter cells through scavenger receptor A mediated endocytosis, without need of any transfection agent.[41] Additionally, ProSNAs combine the functionality of both proteins and nucleic acids in an independent modular format and have been shown to have the potential to be used in applications like functional enzyme delivery and live cell chemical analysis. Since proteins are inherently weakly charged compared to nucleic acids, we hypothesized that higher charge density of the ProSNA complex would amplify the electrophoretic drive and improve the rapid delivery of the protein cargo via electroporation.

To study and quantify this effect, we functionalized the AF-647-tagged β-gal protein with single-stranded DNA tagged with fluorescein isothiocyanate (FITC) at two different surface densities (18 DNA strands/protein (SNA1) and 25 DNA strands/protein (SNA2)). Both sets of ProSNAs were delivered into adhered HeLa cells using the LEPD with the optimized bilevel pulse conditions. The fluorescent micrographs (Figure 3A) show that the ProSNAs were efficiently introduced into most cells (efficiency = 80.25%) in the field of view. In the control case, where the cells in LEPD were incubated with the ProSNAs without any pulsing for the duration of bilevel pulse conditions (~20 s), we did not observe any significant uptake of ProSNAs into the cells (Figure 3A, Figure S3). However, for a much longer incubation

https://doi.org/10.1021/acs.nanolett.2c04374
Nano Lett. 2023, 23, 3653−3660

period (1 h), we did observe internalization of β-gal-SNA into the cells (Figure S3). We next compared the mean fluorescence intensity (MFI) of the AF-647-tagged β-gal bare protein to the two ProSNA constructs delivered via LEPD mediated electroporation. We observed an increase in the average MFI per cell for the ProSNAs compared to the bare β-gal (Figure 3B). Moreover, the uptake of the ProSNA with the higher DNA surface density (SNA2) was significantly higher ($p < 0.05$) than the ProSNA with lower DNA density (SNA1). These results indicate that the negatively charged DNA strands enhance the electrophoretic transport of large proteins into the cytosol.

To determine if the functionality of proteins delivered with the LEPD system is preserved, we used a β-gal activity measurement assay (X-gal) to test for activity of β-gal and β-gal-SNA (SNA2) in the HeLa cells 4 h after delivery. Active β-gal hydrolyzes the X-gal chromogenic substrate, which results in the formation of a blue precipitate that is detectable with optical microscopy. The micrographs we obtained following incubation with X-gal show the presence of the blue precipitate in cells for both bare β-gal and β-gal-SNA, which indicates that the protein remains active in the cells after electroporation (Figure 3C). Furthermore, we obtained images of cells incubated with bare β-gal without application of electric pulses as a negative control and did not observe any blue precipitate following the X-gal assay; therefore, the blue precipitate present in the electroporated cells was a result of the delivered exogenous protein (Figure 3C). We also quantified the X-gal activity for both the β-gal and β-gal-SNA cases by measuring the background-subtracted intensity of the blue precipitate, which yielded higher intensities for the SNA delivered cells compared to the bare β-gal (Figure 3D). The MFI fold change for the SNA relative to the β-gal is in the same order of magnitude as the MFI fold change of the AF647 (see Figure 3B), which indicates that the β-gal enzyme activity is proportional to the amount delivered and demonstrates that the ProSNA's nucleic acid shell does not interfere with the activity of the protein core. It is known that perturbations imparted by the delivery process like changes of pH, protein aggregation, denaturing, or shielding of active sites with secondary molecules may result in conformational changes in proteins and consequent loss of function.[42] Therefore, for proteins to retain their function, the environmental factors imposed on the proteins in the delivery experiment must be carefully considered. Here, the proteins retained their function in the presence of electric fields and after functionalizing their exterior with nucleic acids.

Next, using confocal microscopy, we studied the intracellular localization of β-gal-SNAs following direct delivery with LEPD. For comparison, we delivered linear DNA tagged with FITC in separate LEPDs. The cells were transferred to a confocal dish immediately following electroporation and incubated with the nuclear stain Hoechst 4 h after transfer. Confocal micrographs (Figure 4A) were acquired with different laser lines to excite the three fluorophores covalently coupled to specific locations: β-gal core tagged with AF-647 (red), DNA tagged with FITC (green), and nuclei stained with Hoechst (blue). The images (Figure 4A,B) show a uniform distribution of the ProSNAs within the cytosol of the cells which contrasts the punctate fluorescence that is sometimes characteristic of endocytosis-mediated delivery (Figure S3).[38] Images corresponding to the delivery of the linear DNA strands show that the DNA localizes to the nuclear region (Figure 4A,B, lower panel). We measured the fluorescence intensity along line-segments of select cells for both cases (Figure 4B) to quantify the observations. Indeed, the intensity of the ProSNAs (AF-647 and FITC, Figure 4C (upper panel)) is highest outside the nucleus whereas the free DNA (FITC, Figure 4C (lower panel)) strongly colocalizes to the nucleus. Furthermore, in the case of ProSNAs, there is a strong colocalization between the β-gal protein core and the attached DNA, which indicates that the DNA shell remains attached to the protein core following electroporation. These results indicate that there is a synergistic enhancement of cytosolic delivery efficiency when combining the ProSNA constructs with the multiplexed LEPD platform. These capabilities can allow for the design and execution of *in vitro* studies where ProSNAs can be utilized for sensing cytosolic molecules using DNA (e.g., mRNA detection) or for therapeutic applications (e.g., gene knock-down using antisense oligonucleotides).[6,43]

Following the successful delivery of large protein constructs like β-gal and ProSNA, we evaluated the capability of the LEPD to enable genetic modifications in cells via exogenous protein−RNA complex delivery. The CRISPR-Cas9 system has been extensively used in biomedical research and clinical applications due to its simplicity, ease of use, and precise gene editing capability.[44] The CRISPR-Cas9 gene editing system is typically used in three formats: plasmid DNA, mRNA, and RNP (ribonucleoprotein) complexes. The RNP format uses a preformed complex of the Cas9 protein and the guide RNA which obviates the need for transcription or translation. Therefore, in the RNP format the onset of editing is much faster, avoids the possibility of permanent recombination into the host genome and potential damage to endogenous genes, and is known to have the lowest off-targets effects among all the three formats of delivery.[45−47] Previously, there have been studies where localized electroporation systems were used to successfully deliver Cas9 RNPs into cells bringing about specific genetic modifications.[9,30] However, the genetic modifications attempted were confined to nonhomogenous end-joining (NHEJ) pathways as the data reported contained only the knockout efficiencies. Here we report the capability of the LEPD to successfully deliver a CRISPR-Cas9 based RNP complex along with a single-stranded oligodeoxynucleotide (ssODN) repair template into EGFP expressing K562 cells and bring about a specific homology directed repair (HDR) based genetic modification. Specifically, we used the bilevel pulse shape (P2) and co-delivered a Cas9 RNP complex and a ssODN to knock out the EGFP gene and subsequently introduce a blue fluorescent protein (BFP) encoding gene at the same locus. The knockout efficiency was evaluated for cases where we applied 400, 800, and 1600 P2 pulses to deliver the gene editing cargo. The highest knockout efficiency was observed in the case of 1600 pulses (Figure S4). We also used Lipofectamine (CRISPRmax) to deliver the gene editing cargo; however, the knockout efficiencies were lower than LEPD (Figure S5). Representative phase contrast and fluorescent micrographs in Figure 5A show the successful knock-out of EGFP and knock-in of the BFP expressing gene in many of the K562 cells using the LEPD. We used flow cytometry to quantify the gene editing efficiency (Figure S6), and the data are presented in Figure 5B, where the stacked bar plots represent the percentage of cells that had both BFP knock-in and EGFP knock-out (blue bar), just EGFP knockout (gray bar), and no gene editing (green bar). There was successful knock-in of the BFP gene in 23.6% of the cells, while

https://doi.org/10.1021/acs.nanolett.2c04374
Nano Lett. 2023, 23, 3653−3660

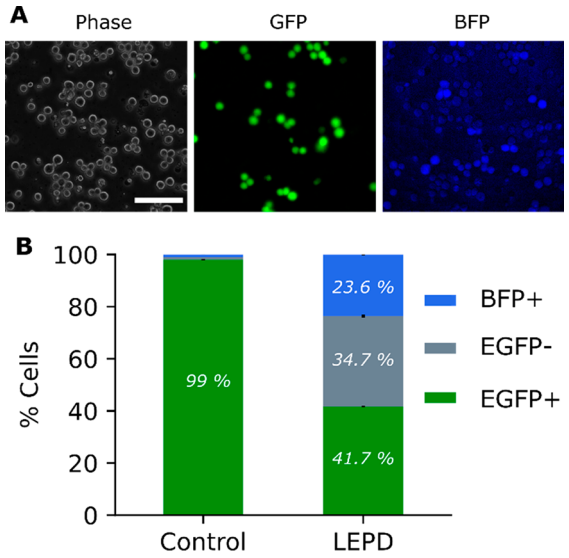

Figure 5. CRISPR/Cas9 delivery and gene editing. (A) Representative phase contrast and fluorescent micrographs of K562 cells, 7 days after CRISPR Cas9-gRNA RNP complex and ssODN delivery. The gRNA targeted the endogenous EGFP, and the ssODN has a BFP template to facilitate homology directed repair (HDR) (left, phase contrast; middle, EGFP; right, BFP). Scale bar = 100 μm. (B) Stacked bar plots of flow cytometry data (Figure S7) to show the average efficiency (N = 3) of knock-out (% of EGFP- cells) and knock-in (% of BFP+ cells). Control refers to untreated cells.

about 34.7% of cells just had EGFP knockout with no knock-in. Therefore, the total editing efficiency was 58.3%, which is substantially higher than previously reported editing efficiencies (25−30%) for localized electroporation systems.[9,30]

In summary we have investigated the cellular delivery of large functional proteins using the multiplexed LEPD system and found that application of a bilevel pulse shape results in superior performance in terms of both delivery efficiency and viability compared to other pulse parameters. Moreover, we observed that the efficiency and dosage are improved by using ProSNAs compared to bare protein, even though the ProSNA conjugate is substantially larger. We hypothesize that the charged DNA strands of the ProSNA enhance electrophoretic transport, leading to increased molecular delivery into the cell's interior. Moreover, we used a protein activity assay to show that both the bare protein and the ProSNA retain their activity after delivery, which indicates that the employed pulse parameters and experimental conditions do not compromise the protein functionality. We also characterized intracellular localization of the delivered molecules and observed that DNA delivered using the ProSNA architecture is mostly homogeneously distributed in the cytoplasm as opposed to linear DNA, which is localized to the nucleus after delivery. Furthermore, as an application of protein delivery, we delivered a CRISPR Cas9-gRNA RNP complex along with a ssODN to knock out EGFP and subsequently knock in BFP in K562 cells with higher editing efficiencies than previously reported for localized electroporation systems.

This work expands the capabilities of nanochannel membrane based electroporation devices previously demonstrated by Espinosa et al.[28] and others,[9] by increasing the multiplexing capacity and throughput using the well-plate architecture. A high-throughput platform with multiplexing is essential for optimizing electroporation experiments due to the vast number of experimental variables (e.g., pulse parameters, various cell types, buffers, molecular cargos, etc.). Here, the multiplexed design of the LEPD along with AI assisted image analysis was used to quickly optimize the pulse conditions for delivering large proteins and protein-based constructs. Moreover, this work shows that in addition to previous demonstrations of the LEPD that were confined to the delivery of highly charged species like plasmids and small molecules like siRNA,[8] the LEPD can also be used for direct delivery of large proteins into the cytosol, while retaining protein functionality, without being dependent on secondary mechanisms like endosomal escape, which is an issue with most chemical carriers. Furthermore, the study demonstrates that the LEPD technology is capable of leveraging engineered nanostructures like ProSNAs to enhance molecular delivery and, as a result, can potentially be used in cell engineering workflows that entail delivery of large protein complexes like CRISPR-RNP to carry out CRISPR-mediated gene editing.

■ ASSOCIATED CONTENT

Supporting Information

The Supporting Information is available free of charge at https://pubs.acs.org/doi/10.1021/acs.nanolett.2c04374.

Materials and methods section detailing device fabrication and assembly, cell culture, cell seeding, electroporation protocol, automated imaging and AI segmentation, confocal microscopy, DNA synthesis and characterization, ProSNA synthesis and characterization, β-gal and ProSNA delivery with LEPD and activity assay, CRISPR Cas9 RNP preparation protocol, lipofectamine protocol, flow cytometry analysis, statistical analysis; figures showing fluorescent images of cells with β-gal and SNA delivered for pulse optimization, representative confocal micrographs of HeLa cells in LEPD incubated with β-gal-SNA, EGFP knockout using LEPD, EGFP knockout using lipofectamine, flow cytometry analysis data; references (PDF)

■ AUTHOR INFORMATION

Corresponding Author

Horacio D. Espinosa − *Department of Mechanical Engineering and Theoretical and Applied Mechanics Program, Northwestern University, Evanston, Illinois 60208, United States;* orcid.org/0000-0002-1907-3213; Email: espinosa@northwestern.edu

Authors

Nibir Pathak − *Department of Mechanical Engineering and Theoretical and Applied Mechanics Program, Northwestern University, Evanston, Illinois 60208, United States*

Cesar A. Patino − *Department of Mechanical Engineering, Northwestern University, Evanston, Illinois 60208, United States;* orcid.org/0000-0003-3074-9314

Namrata Ramani − *Department of Materials Science and Engineering and International Institute for Nanotechnology, Northwestern University, Evanston, Illinois 60208, United States*

Prithvijit Mukherjee − *Department of Mechanical Engineering and Theoretical and Applied Mechanics Program, Northwestern University, Evanston, Illinois 60208, United States*

https://doi.org/10.1021/acs.nanolett.2c04374
Nano Lett. 2023, 23, 3653−3660

Devleena Samanta − *Department of Chemistry and International Institute for Nanotechnology, Northwestern University, Evanston, Illinois 60208, United States*

Sasha B. Ebrahimi − *Department of Chemical and Biological Engineering and International Institute for Nanotechnology, Northwestern University, Evanston, Illinois 60208, United States;* orcid.org/0000-0003-2752-5109

Chad A. Mirkin − *Department of Chemistry and International Institute for Nanotechnology, Northwestern University, Evanston, Illinois 60208, United States;* orcid.org/0000-0002-6634-7627

Complete contact information is available at: https://pubs.acs.org/10.1021/acs.nanolett.2c04374

Author Contributions

#N.P. and C.A.P. contributed equally to this work. The manuscript was written through contributions of all authors. All authors have given approval to the final version of the manuscript. H.D.E. and C.A.M. conceived the project and provided overall guidance. N.P. and C.A.P. fabricated the devices, designed and performed the delivery experiments, and processed experimental outcomes. N.R. performed the activity assays and confocal imaging. P.M. contributed to designing and carrying out the CRISPR mediated gene editing experiments. D.S. and S.B.E. designed the ProSNAs and provided motivation and guidance on experiments with ProSNA and DNA delivery. All the authors analyzed the data and provided inputs for the discussion.

Notes

The authors declare no competing financial interest.

■ ACKNOWLEDGMENTS

Research reported in this publication was supported by the NIH R21 Award 8041R21GM132709-01, the National Science Foundation Grant DBI-2032180, and the United States Air Force (subaward from TERA-print, LLC) Award FA9550-18-1-0493. S.B.E. was supported in part by the Chicago Cancer Baseball Charities and the H Foundation at the Lurie Cancer Center of Northwestern University.

■ REFERENCES

(1) Leader, B.; Baca, Q. J.; Golan, D. E. Protein therapeutics: a summary and pharmacological classification. *Nat. Rev. Drug Discovery* **2008**, *7* (1), 21−39.

(2) Huang, C.; Han, Z.; Evangelopoulos, M.; Mirkin, C. A. CRISPR Spherical Nucleic Acids. *J. Am. Chem. Soc.* **2022**, *144* (41), 18756−18760.

(3) Mout, R.; Ray, M.; Yesilbag Tonga, G.; Lee, Y.-W.; Tay, T.; Sasaki, K.; Rotello, V. M. Direct Cytosolic Delivery of CRISPR/Cas9-Ribonucleoprotein for Efficient Gene Editing. *ACS Nano* **2017**, *11* (3), 2452−2458.

(4) Bailus, B. J.; Pyles, B.; McAlister, M. M.; O'Geen, H.; Lockwood, S. H.; Adams, A. N.; Nguyen, J. T. T.; Yu, A.; Berman, R. F.; Segal, D. J. Protein Delivery of an Artificial Transcription Factor Restores Widespread Ube3a Expression in an Angelman Syndrome Mouse Brain. *Molecular Therapy* **2016**, *24* (3), 548−555.

(5) Stewart, M. P.; Langer, R.; Jensen, K. F. Intracellular Delivery by Membrane Disruption: Mechanisms, Strategies, and Concepts. *Chem. Rev.* **2018**, *118* (16), 7409−7531.

(6) Samanta, D.; Ebrahimi, S. B.; Kusmierz, C. D.; Cheng, H. F.; Mirkin, C. A. Protein spherical nucleic acids for live-cell chemical analysis. *J. Am. Chem. Soc.* **2020**, *142* (31), 13350−13355.

(7) Marschall, A. L. J.; Zhang, C.; Frenzel, A.; Schirrmann, T.; Hust, M.; Perez, F.; Dübel, S. Delivery of antibodies to the cytosol. *mAbs* **2014**, *6* (4), 943−956.

(8) Patino, C. A.; Pathak, N.; Mukherjee, P.; Park, S. H.; Bao, G.; Espinosa, H. D. Multiplexed high-throughput localized electroporation workflow with deep learning-based analysis for cell engineering. *Sci. Adv.* **2022**, *8* (29), eabn7637.

(9) Cao, Y.; Ma, E.; Cestellos-Blanco, S.; Zhang, B.; Qiu, R.; Su, Y.; Doudna, J. A.; Yang, P. Nontoxic nanopore electroporation for effective intracellular delivery of biological macromolecules. *Proc. Natl. Acad. Sci. U. S. A.* **2019**, *116* (16), 7899−7904.

(10) Schmiderer, L.; Subramaniam, A.; Žemaitis, K.; Bäckström, A.; Yudovich, D.; Soboleva, S.; Galeev, R.; Prinz, C. N.; Larsson, J.; Hjort, M. Efficient and nontoxic biomolecule delivery to primary human hematopoietic stem cells using nanostraws. *Proc. Natl. Acad. Sci. U. S. A.* **2020**, *117* (35), 21267−21273.

(11) Nathamgari, S. S. P.; Pathak, N.; Lemaitre, V.; Mukherjee, P.; Muldoon, J. J.; Peng, C. Y.; McGuire, T.; Leonard, J. N.; Kessler, J. A.; Espinosa, H. D. Nanofountain Probe Electroporation Enables Versatile Single-Cell Intracellular Delivery and Investigation of Postpulse Electropore Dynamics. *Small* **2020**, *16* (43), 2002616.

(12) Patino, C. A.; Mukherjee, P.; Berns, E. J.; Moully, E. H.; Stan, L.; Mrksich, M.; Espinosa, H. D. High-Throughput Microfluidics Platform for Intracellular Delivery and Sampling of Biomolecules from Live Cells. *ACS Nano* **2022**, *16* (5), 7937−7946.

(13) Sharei, A.; Zoldan, J.; Adamo, A.; Sim, W. Y.; Cho, N.; Jackson, E.; Mao, S.; Schneider, S.; Han, M.-J.; Lytton-Jean, A.; Basto, P. A.; Jhunjhunwala, S.; Lee, J.; Heller, D. A.; Kang, J. W.; Hartoularos, G. C.; Kim, K.-S.; Anderson, D. G.; Langer, R.; Jensen, K. F. A vector-free microfluidic platform for intracellular delivery. *Proc. Natl. Acad. Sci. U.S.A.* **2013**, *110* (6), 2082−2087.

(14) Ding, X.; Stewart, M. P.; Sharei, A.; Weaver, J. C.; Langer, R. S.; Jensen, K. F. High-throughput nuclear delivery and rapid expression of DNA via mechanical and electrical cell-membrane disruption. *Nat. Biomed. Eng.* **2017**, *1* (3), 0039.

(15) Joo, B.; Hur, J.; Kim, G.-B.; Yun, S. G.; Chung, A. J. Highly Efficient Transfection of Human Primary T Lymphocytes Using Droplet-Enabled Mechanoporation. *ACS Nano* **2021**, *15* (8), 12888−12898.

(16) Hur, J.; Park, I.; Lim, K. M.; Doh, J.; Cho, S.-G.; Chung, A. J. Microfluidic cell stretching for highly effective gene delivery into hard-to-transfect primary cells. *ACS Nano* **2020**, *14* (11), 15094−15106.

(17) Kang, G.; Carlson, D. W.; Kang, T. H.; Lee, S.; Haward, S. J.; Choi, I.; Shen, A. Q.; Chung, A. J. Intracellular Nanomaterial Delivery via Spiral Hydroporation. *ACS Nano* **2020**, *14* (3), 3048−3058.

(18) Felgner, P. L.; Gadek, T. R.; Holm, M.; Roman, R.; Chan, H. W.; Wenz, M.; Northrop, J. P.; Ringold, G. M.; Danielsen, M. Lipofection: a highly efficient, lipid-mediated DNA-transfection procedure. *Proc. Natl. Acad. Sci. U. S. A.* **1987**, *84* (21), 7413−7417.

(19) Zeitelhofer, M.; Vessey, J. P.; Xie, Y.; Tübing, F.; Thomas, S.; Kiebler, M.; Dahm, R. High-efficiency transfection of mammalian neurons via nucleofection. *Nature protocols* **2007**, *2* (7), 1692−1704.

(20) Ebrahimi, S. B.; Samanta, D.; Kusmierz, C. D.; Mirkin, C. A. Protein transfection via spherical nucleic acids. *Nat. Protoc.* **2022**, *17* (2), 327−357.

(21) Distler, M. E.; Teplensky, M. H.; Bujold, K. E.; Kusmierz, C. D.; Evangelopoulos, M.; Mirkin, C. A. DNA Dendrons as Agents for Intracellular Delivery. *J. Am. Chem. Soc.* **2021**, *143* (34), 13513−13518.

(22) Säälik, P.; Elmquist, A.; Hansen, M.; Padari, K.; Saar, K.; Viht, K.; Langel, Ü.; Pooga, M. Protein Cargo Delivery Properties of Cell-Penetrating Peptides. A Comparative Study. *Bioconjugate Chem.* **2004**, *15* (6), 1246−1253.

(23) Mix, K. A.; Lomax, J. E.; Raines, R. T. Cytosolic Delivery of Proteins by Bioreversible Esterification. *J. Am. Chem. Soc.* **2017**, *139*, 1520−5126.

(24) Lv, J.; Wang, H.; Rong, G.; Cheng, Y. Fluorination Promotes the Cytosolic Delivery of Genes, Proteins, and Peptides. *Acc. Chem. Res.* **2022**, *55* (5), 722−733.

(25) Cheng, Y. Design of Polymers for Intracellular Protein and Peptide Delivery. *Chin. J. Chem.* **2021**, *39* (6), 1443−1449.
(26) Lv, J.; Fan, Q.; Wang, H.; Cheng, Y. Polymers for cytosolic protein delivery. *Biomaterials* **2019**, *218*, 119358.
(27) Stewart, M. P.; Sharei, A.; Ding, X.; Sahay, G.; Langer, R.; Jensen, K. F. In vitro and ex vivo strategies for intracellular delivery. *Nature* **2016**, *538* (7624), 183−192.
(28) Mukherjee, P.; Nathamgari, S. S. P.; Kessler, J. A.; Espinosa, H. D. Combined Numerical and Experimental Investigation of Localized Electroporation-Based Cell Transfection and Sampling. *ACS Nano* **2018**, *12* (12), 12118−12128.
(29) Son, R. S.; Smith, K. C.; Gowrishankar, T. R.; Vernier, P. T.; Weaver, J. C. Basic features of a cell electroporation model: illustrative behavior for two very different pulses. *J. Membr. Biol.* **2014**, *247* (12), 1209−28.
(30) Cao, Y.; Chen, H.; Qiu, R.; Hanna, M.; Ma, E.; Hjort, M.; Zhang, A.; Lewis, R. S.; Wu, J. C.; Melosh, N. A. Universal intracellular biomolecule delivery with precise dosage control. *Sci. Adv.* **2018**, *4* (10), eaat8131.
(31) Falk, T.; Mai, D.; Bensch, R.; Çiçek, Ö.; Abdulkadir, A.; Marrakchi, Y.; Böhm, A.; Deubner, J.; Jäckel, Z.; Seiwald, K.; et al. U-Net: deep learning for cell counting, detection, and morphometry. *Nat. Methods* **2019**, *16* (1), 67.
(32) Carpenter, A. E.; Jones, T. R.; Lamprecht, M. R.; Clarke, C.; Kang, I. H.; Friman, O.; Guertin, D. A.; Chang, J. H.; Lindquist, R. A.; Moffat, J.; et al. CellProfiler: image analysis software for identifying and quantifying cell phenotypes. *Genome Biol.* **2006**, *7* (10), R100.
(33) Patino, C. A.; Mukherjee, P.; Lemaitre, V.; Pathak, N.; Espinosa, H. D. Deep Learning and Computer Vision Strategies for Automated Gene Editing with a Single-Cell Electroporation Platform. *SLAS Technol.* **2021**, *26* (1), 26−36.
(34) Mukherjee, P.; Patino, C. A.; Pathak, N.; Lemaitre, V.; Espinosa, H. D. Deep Learning-Assisted Automated Single Cell Electroporation Platform for Effective Genetic Manipulation of Hard-to-Transfect Cells. *Small* **2022**, *18* (20), 2107795.
(35) Kotnik, T.; Rems, L.; Tarek, M.; Miklavčič, D. Membrane Electroporation and Electropermeabilization: Mechanisms and Models. *Annu. Rev. Biophys* **2019**, *48*, 63−91.
(36) Melikov, K. C.; Frolov, V. A.; Shcherbakov, A.; Samsonov, A. V.; Chizmadzhev, Y. A.; Chernomordik, L. V. Voltage-induced nonconductive pre-pores and metastable single pores in unmodified planar lipid bilayer. *Biophys. J.* **2001**, *80* (4), 1829−36.
(37) Kotnik, T.; Pucihar, G.; Miklavčič, D. Induced Transmembrane Voltage and Its Correlation with Electroporation-Mediated Molecular Transport. *J. Membr. Biol.* **2010**, *236* (1), 3−13.
(38) Brodin, J. D.; Sprangers, A. J.; McMillan, J. R.; Mirkin, C. A. DNA-mediated cellular delivery of functional enzymes. *J. Am. Chem. Soc.* **2015**, *137* (47), 14838−14841.
(39) Kusmierz, C. D.; Bujold, K. E.; Callmann, C. E.; Mirkin, C. A. Defining the design parameters for in vivo enzyme delivery through protein spherical nucleic acids. *ACS central science* **2020**, *6* (5), 815−822.
(40) Batista Napotnik, T.; Polajžer, T.; Miklavčič, D. Cell death due to electroporation − A review. *Bioelectrochemistry* **2021**, *141*, 107871.
(41) Choi, C. H. J.; Hao, L.; Narayan, S. P.; Auyeung, E.; Mirkin, C. A. Mechanism for the endocytosis of spherical nucleic acid nanoparticle conjugates. *Proc. Natl. Acad. Sci. U. S. A.* **2013**, *110* (19), 7625−7630.
(42) Frokjaer, S.; Otzen, D. E. Protein drug stability: a formulation challenge. *Nat. Rev. Drug Discovery* **2005**, *4* (4), 298−306.
(43) Ebrahimi, S. B.; Samanta, D.; Cheng, H. F.; Nathan, L. I.; Mirkin, C. A. Forced Intercalation (FIT)-Aptamers. *J. Am. Chem. Soc.* **2019**, *141* (35), 13744−13748.
(44) Kim, S.; Kim, D.; Cho, S. W.; Kim, J.; Kim, J.-S. Highly efficient RNA-guided genome editing in human cells via delivery of purified Cas9 ribonucleoproteins. *Genome research* **2014**, *24* (6), 1012−1019.
(45) Fajrial, A. K.; He, Q. Q.; Wirusanti, N. I.; Slansky, J. E.; Ding, X. A review of emerging physical transfection methods for CRISPR/Cas9-mediated gene editing. *Theranostics* **2020**, *10*, 5532−5549.
(46) Lin, S.; Staahl, B. T.; Alla, R. K.; Doudna, J. A. Enhanced homology-directed human genome engineering by controlled timing of CRISPR/Cas9 delivery. *eLife* **2014**, *3*, e04766.
(47) Chen, S.; Sun, S.; Moonen, D.; Lee, C.; Lee, A. Y.-F.; Schaffer, D. V.; He, L. CRISPR-READI: Efficient generation of knockin mice by CRISPR RNP electroporation and AAV donor infection. *Cell Rep.* **2019**, *27* (13), 3780−3789.

https://doi.org/10.1021/acs.nanolett.2c04374
Nano Lett. 2023, 23, 3653−3660